ELASTO-MECHANICAL CHARACTERIZATION OF SOLID-LIQUID COMPOSITES

by

Karthik Kundapur

A Thesis Submitted in Partial Fulfillment

of the Requirements for the Degree

Master's in Engineering

Major Subject: Mechanical Engineering

West Texas A&M University

Canyon, Texas

November 2023

Abstract

Solid-liquid composites (SLCs) are a class of soft materials with soft solid matrix encapsulating liquid inclusions. These novel composite materials have a wide range of potential applications, including thermal management, biomedicine, soft-robotics, and flexible electronics [1], [2]. By manipulating the type and volume of the liquid inclusion, the properties of SLCs can be fine-tuned to suit specific requirements. In this work, a dilute SLC is developed using commercial grade silicone (Smoothon Ecoflex 00-30) as the solid phase and laboratory-grade Glycerin as the liquid inclusion. While Eco-flex 00-30 mimics the behavior of a certain class of human tissues [3], Glycerin was selected as it is non-toxic and immiscible with silicone. A *novel fabrication technique* was developed for the precise distribution of the liquid inclusion in the soft polymeric material. The elastic properties of the SLCs were then determined experimentally for various volume fractions of the inclusion phase. The experimental data was then used to characterize the linear-elastic and hyperelastic material properties. The fabricated SLCs are also shown to exhibit properties similar to biofidelic materials from literature.

Acknowledgements

I wish to express my deep appreciation to my advisor, Dr. Vinu Unnikrishnan, for invaluable guidance at every phase of this research, and to Dr. Fisseha M. Alemayehu and Dr. Anitha Subburaj for agreeing to be part of my committee and for their time spent reviewing my work. Your wealth of knowledge, constructive critiques, and thought-provoking suggestions have continuously spurred me to engage critically and strive for excellence. Your unswerving dedication to my academic progress has played a pivotal role in the completion of this thesis.

I am also thankful to Dr. Pamela Lockwood, College of Engineering, West Texas A&M University for supporting me with Graduate Research Assistantship. The university's abundant resources, state-of-the-art facilities, and expert faculty have significantly contributed to facilitating my research endeavors.

My gratitude extends to my family and friends whose steadfast encouragement and boundless motivation have been my pillars of strength throughout my academic journey.

Approved:

Dr. Vinu Unnikrishnan
Chairman, Thesis Committee 11/08/2023

Dr. Fisseha M. Alemayehu
Member, Thesis Committee 11/08/2023

Dr. Anitha Subburaj
Member, Thesis Committee 11/08/2023

[Department Head/Direct Supervisor] [Date]

[Dean, Academic College] [Date]

[Dean, Graduate School] [Date]

Table of Contents

List of Figures

List of Tables

Chapter 1: Introduction

1.1 Introduction to Solid-Liquid Composites (SLCs):

A composite material can be defined as the assembly of two or more materials, the final assembly having properties superior to the properties of each of the constituent materials [4]. These components work together to enhance material properties that wouldn't be achievable with individual materials alone. Composites are classified based on various criteria like hardness, softness, and phase composition and it can be categorized in multiple ways. In this work, it is broadly classified into hard composites and soft composites.

Hard composites are made by mixing a strong, rigid material with a tougher, less flexible material which is characterized by structural rigidity and strong (e.g., covalent or ionic) interactions [5], examples: carbon fiber-reinforced polymer composites and ceramic matrix composites.

Soft matter possesses properties in between solids and liquids and is dominated by weaker, intermolecular interactions (e.g., dipolar or hydrogen bonding interactions) [5]. They often display flexible and deformable properties, allowing them to undergo various mechanical changes while maintaining their overall integrity. They are often used in

applications requiring conformability and impact absorption, such as protective gear, medical devices, and soft robotics.

Solid-liquid composites (SLCs) are a special group of soft materials blending solids and liquids (Figure 1). They're gaining prominence in materials science. SLCs consist of distinct phases: a solid structure and a liquid component. These phases are combined strategically to achieve desired properties of the material. The solid part provides stability and shape, encapsulating the liquid phase. Meanwhile, the liquid element, such as water, liquid metals, or complex fluids provide flexibility and adaptability, making SLCs highly versatile in various technical applications, these properties are a result of dramatically different properties of the liquid and solid phases [2].

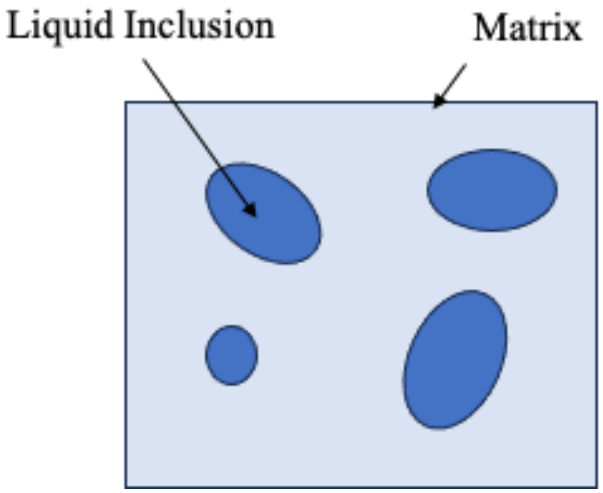

Figure 1: Schematic of a solid-liquid composite system.

The solid component often determines the mechanical strength and overall structure of the composite, while the liquid component adds various functionalities. By adjusting the volume fraction of the liquid content, the properties of the composites can be tailored, resulting in versatile, durable materials customized to specific needs.

Due to their soft yet functional response, they are ideal for soft robotics, soft actuation, and soft electronics where soft components replace traditionally rigid components to achieve high levels of deformability and compliance [6]. SLCs not only exhibit exceptional static physical properties but also demonstrate remarkable dynamic impact resistance to meet the demands of intricate real-world scenarios such as drops and impacts [7]. Having the ability to simultaneously exhibit high strength and toughness, SLCs have a combination of mechanical properties that were traditionally seen as incompatible [8]. In typical composites, a compromise must be made between toughness and stiffness where one is improved at the expense of the other [9].

On the contrary, nature has examples where both the properties are in optimum, for instance, the intervertebral discs (Figure 2) that separate spinal cord vertebrae, consists of an inner liquid nucleus (nucleus pulposus) surrounded by a tough outer coating and Type I collagen (annulus fibrous) [10], [11]. They act as efficient shock absorbers to prevent fractures of the vertebrae due to compression loading and provide mobility to the spine, allowing it to bend and twist with minimal damage. These adaptations allow the disc to sustain very high stress by utilizing liquid components [9].

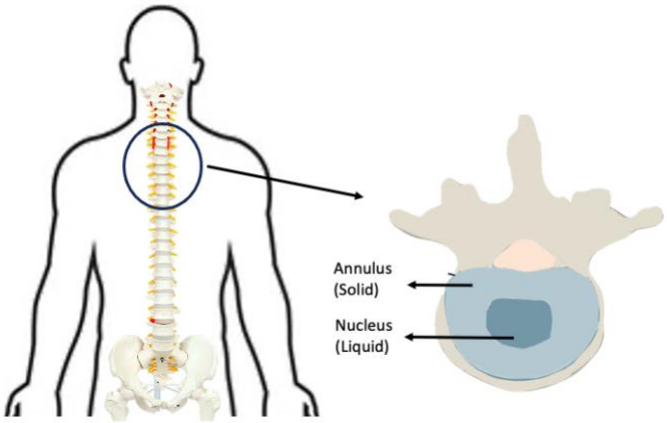

Figure 2: Human intervertebral disk- an example of naturally present SLC.

New combinations of soft materials and fluids can result in distinct and advantageous properties. One approach involves incorporating specialized fluids like liquid metals (LMs) and ferrofluids into soft elastomers. This integration imparts the composite with the liquid's unique characteristics, such as electrical conductivity, thermal conductivity, magnetic responsiveness, or actuation ability – properties that are usually weak in soft solids. Remarkably, these enhancements are achieved while preserving the soft and deformable properties of the elastomer phase [2].

1.2 Classification of Solid Liquid Composites:

SLCs can be classified based on their morphology into macro-structured and micro-structured. Macro-structured (Figure 3a) SLCs are composed of a solid matrix infused with a liquid phase, with the solid component being load-bearing, and the liquid component filling in the voids and providing additional properties such as flexibility, conductivity, or reactivity [9]. Micro-structured (Figure 3b) SLCs have a homogeneous distribution of solid and liquid phases that are intimately mixed at the nanometer or micrometer scales [12], [13].

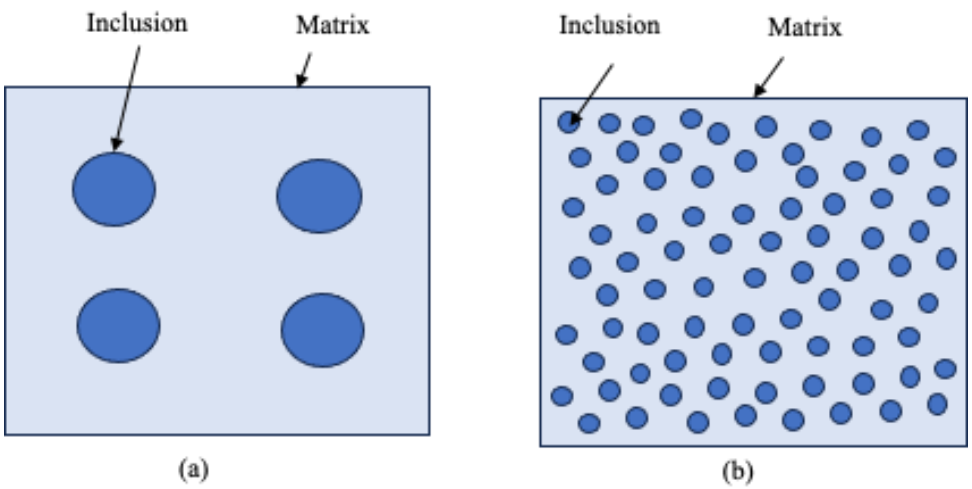

Figure 3: Schematic of classification of SLCs based on morphology (a) Macrostructured SLC, (b) Microstructured SLC.

Based on spatial dimensionality SLCs are classified as [14] (Figure 4):

- **0D:** SLCs are in the form of discrete particles.
- **1D:** SLCs form linear structures.
- **2D:** SLCs form a thin layer/sheet.
- **3D:** SLCs form a three-dimensional structure.

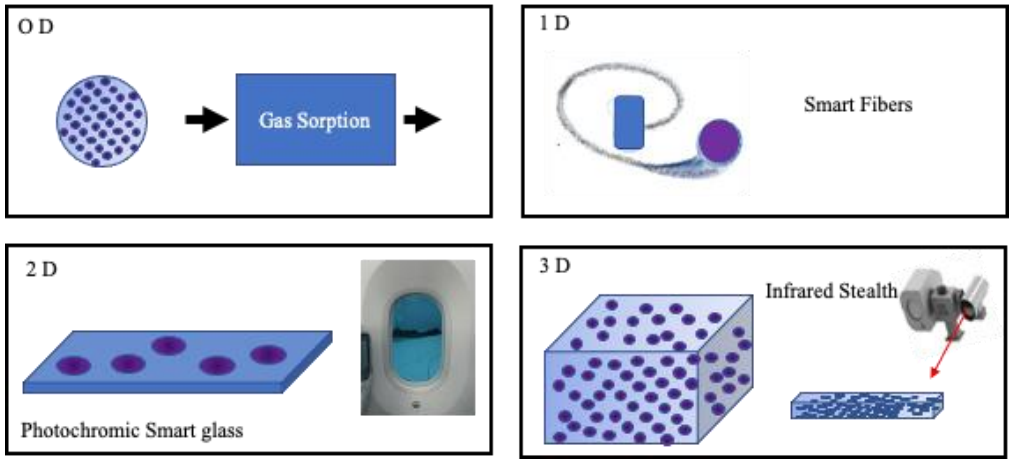

Figure 4: Schematic of classification of SLCs based on spatial dimensionality.

1.3 Applications of Solid Liquid Composites:

Solid-liquid composites (SLCs) have many potential applications across a range of fields. For instance, SLCs can be used as smart drug delivery systems and as biofidelic human tissue surrogates [2], [15], [16], [17], [18], [19]. They can be used as thermal storage devices, such that the SLCs made of Phase Change Materials (PCMs) transition between solid and liquid phases allowing for efficient storage and release of thermal energy [20]–[22]. Additionally, SLCs have been used in the development of sensing devices by taking advantage of their unique mechanical and functional properties [23]. Due to their ability to undergo deformation and return to initial condition in response to external stimuli, SLCs are used as actuators in soft robotics [2], [24], [25]. Furthermore, liquid metal-polymer composites based SLCs, have potential applications in flexible electronics, enabling stretching without losing functionality [16], [20]. SLCs containing liquid metals have been used to create conductive materials in electronics, circuitry, and interconnects [16], [26]. In material science and engineering, SLCs are used as coatings to provide enhanced properties, such as improved wear resistance, corrosion resistance, and self-healing capabilities [2]. In addition, SLCs are used for impact resistance, where they have shown enhanced performance in redistributing cracks and absorbing energy under dynamic loading conditions [27].

1.4 Choice of Solid and Liquid Medium:

In solid-liquid composites, multifunctional properties can be achieved by the use of different fluids as liquid inclusions. These liquid inclusions play an important role and contribute significantly to the overall composite's behavior. Different liquids such as metallic, aqueous, hydrocarbons, silicones, fluorocarbons, and ionic liquids, are selected

based on their inherent properties [2]. For example, liquids typically containing iron particles suspended in a carrier liquid to create ferrofluids or Magnetorheological Fluids (MRFs) are used for desired magnetic responses. For electrical conductivity applications, conductive liquids, such as LMs, ionic liquids, and salt solutions are preferred, here, LMs ensure efficient transmission of electrical signals [28]. For applications which require enhanced thermal conductivity, LMs offer the highest conductivity when a magnetic field is applied, MRFs have also been used to enhance conductivity as the particles of the MRF's align to create conductive chains [29]. For toughening effects, LMs have demonstrated a generic toughening effect on the properties of soft composites.[16], [30]. For biomedical applications, fluorinated oil and silicone oil are excellent choices as they are biocompatible, chemically stable, and non-flammable [31], [32].

While the choice of a suitable liquid medium is relatively diverse, choices in selection of solid matrix are significantly limited. The selection of an appropriate solid matrix depends on various factors, starting with compatibility with the chosen liquid. Furthermore, factors such as stiffness, extensibility, fracture resistance, toughness, temperature stability, and cost play major roles in the decision-making process. Among the most frequently utilized solid matrix materials are silicones, polyurethanes, thermoplastic elastomers like Styrene Isoprene Rubbers (SIS), and hydrogels. These materials are favored due to their unique combination of properties, making them ideal candidates for creating advanced solid-liquid composites.

1.5 Literature Review and Background:

There are numerous studies in literature for the **estimation** of mechanical properties of SLCs using experimental and analytical techniques. Most of the experimental studies are based on uniaxial tensile testing, and majority of the analytical studies are based on the linear elastic behavior of the components of the SLCs. Since majority of the SLCs are soft composite materials, they exhibit strong hyperelastic behavior. Currently, there are very few studies that focus on the hyperelastic-based material characterization.

Experimental studies by Style et al. [13] showed the stiffening of SLCs using liquid Glycerin droplets embedded in a soft silicone matrix where the stiffening was proportional to the increase in the volume fraction of the liquids. This study also showed that there is a loss of effective stiffness with an increase in the volume fraction of the inclusion when embedded in a stiff matrix. While studies by Mathias et al. [12] showed a decrease in effective Young's Modulus of the SLCs with an increase in the volume fraction, Owuor et al. [9] showed that the use of liquid Gallium metal as inclusions in compliant elastomer polydimethylsiloxane (PDMS) led to high stiffness and high energy absorption in the composite even with larger inclusion sizes. Extreme toughening effects were witnessed in an experimental study carried out by Kazem et al. [16]. Here, the presence of liquid inclusions eliminated crack dissipation when stretched uniaxially. The study by Yu et al. [27] investigates solid-liquid composites created through microfluidic 3D printing, featuring functional liquid inclusions. These SLCs, vital for smart

electronics and soft robotics, were tested using dynamic split-Hopkinson pressure bar (SHPB). These experimental studies indicated enhanced impact resistance and energy dissipation compared to pure materials. Another study by Fei et al.[33] with cylindrical shaped liquid inclusion investigates the impact of surface effects on the elastic field and mechanical properties of microscale liquid-filled channels in biological tissues. This study proposed a theoretical model accounting for surface curvature together with Eshelby's formalism and estimated the effective mechanical properties of composites containing liquid-filled microchannels. The study revealed that surface effects prevent deformation of the liquid inclusion and increase stress concentration around the interphase. In an analytical study by Wu et al. [34] focusing on elliptical compressible liquid inclusion, addresses the role of liquid pressure changes during the deformation of the inclusion. The study showed that liquid pressure change and surface tension, enhances the effective plane-strain Young's Modulus of a solid-liquid composite system. A study by Hamidia et al. [35] employed three stochastic and two deterministic models to determine the effective Young's Modulus of the composites with liquid inclusion and soft matrix, focusing on elasto-capillary coupling phenomena. The findings highlighted the dominant roles of inclusion size and surface tension, the changing influence of volume fraction on material properties, and the importance of considering interactions between factors like agglomeration and model selection.

Various analytical models in literature focus on characterizing the mechanical properties of solid-liquid composites using Eshelby's theory [13]. Style et al [13] showed that the composite becomes softer as the liquid content increases for a stiffer matrix. Additionally, this study also considered the effect of surface stresses and capillary effects

on the mechanical properties of the solid-liquid composites. Similarly, Eshelby's theory was extended by Sharma et al. [36] to present explicit expressions for the modified Eshelby tensor focusing on spherical and cylindrical inclusions considering surface stress effects. Krichen et al. [37] extended the Gurtin-Murdoch surface elasticity theory to include the surface stress effects which in the dilute limit, matches the analytical model by Style et al. [13]. In the same study, when the surface tension becomes negligible, the composite becomes more compliant in exact agreement with Eshelby's prediction [13]. Mancarella et al. [38] within the framework of Mori-Tanaka multiphase approximation scheme, extended Eshelby's theory to a composite with interfacial stresses in the non-dilute limit. The study predicts that the composite stiffness depends strongly on the ratio of the droplet size, $\boldsymbol{R}$, to the elastocapillary length scale, $\boldsymbol{L}$. In a similar study without involving the solid-liquid composites, traditional micro mechanical models were used by Yun et al. [39] to predict elastic properties of the composite and the results were compared with finite element analysis, the study used simple mechanics models like Voigt Model, Reuss Model, and Halpin–Tsai Model to estimate the elastic properties of a composite made using ultra-high molecular weight polyethylene (UHMWPE) spherical molecules in a polypropylene (PP) matrix. The study highlighted the limitations of these models which involves various assumption like homogeneity, ignoring the microstructural details and thus can be applied to only certain types of composites. Therefore, models that take into consideration the microstructural details of the inclusion phases are required for predicting the properties of SLCs**.**

SLCs with soft polymer matrices exhibit large nonlinear deformations under loading and hence a hyperplastic material-based characterization enables a better

characterization of the material behavior [40]. There are some related studies that deal with the application of hyperplastic material behavior, but most have been on ionic gels, biofidelic materials, and soft tissues [41], [42], [43]. Bin He at al. [42] applied Mooney-Rivlin model to describe the mechanical behavior of ionic liquid gels, with hard inclusions. Another study by Weizel et al. [41] used several models including Ogden and Mooney-Rivlin models to characterize the mechanical behavior of cartilage and surrogate materials (ADA-GEL and ChondroFiller). Park et al. developed a pressure transducer by embedding silicone rubber with microchannels of eutectic Gallium–Indium liquid and characterized its mechanical behavior using hyperelastic material models [44]. Recently, Ghosh and Lopez-Pamies [45] developed a formulation using homogenization based macroscopic mechanical behavior of elastomeric materials filled with liquid inclusions under finite quasi-static deformations. Heyden et al. [46] also developed a mean-field homogenization of swollen elastomers with hyperelastic matrix and microgel inclusions. Thus, there has been very limited work in literature that directly characterizes the mechanical properties of the SLCs made of soft polymeric materials and more specifically silicone-based polymers with Glycerin inclusions.

1.6 Challenges in the Fabrication of SLC Systems:

Generally, the fabrication of SLCs is complex because of the challenges associated with handling liquid inclusions. As a result, there are significant hurdles in developing a simple and efficient fabrication technique for SLCs.

Style et al. [13] employed the spin coat method, utilizing a dilute mixture of silicone and glycerol. In a different approach, Owuor et al. [9] used Gallium inclusions on

a semi-cured layer of PDMS, followed by the pouring of a second layer of PDMS. Using Gallium as an inclusion offers an advantage in that unlike Glycerin, Gallium remains in a solid state at room temperature.

In a polymeric matrix-based solid-liquid composite (SLC) system, a crucial challenge arises during the initial stages of fabrication. Inclusions must be seamlessly integrated into the matrix before the polymerization process commences. The difficulty lies in ensuring that the liquid inclusions are to be suspended at the required height within the matrix thickness, which naturally tends to settle due to gravitational forces. Existing research have explored the use of surfactants to assist in retaining the inclusions in their designated positions. However, these surfactants often influence and tend to interfere with the overall properties of the composite [47].

Thus, this research focuses on addressing the limitations associated with the fabrication of solid-liquid composites (SLCs) and providing a better analytical characterization using Eshelby's formalism and hyperelastic material models. A novelty of the current work is on the development of an innovative approach in fabricating SLCs that does not rely on surfactants which are typically used to stabilize inclusions. In this work, the position and size of the liquid inclusions within the composite material are precisely controlled without the risk of sinking or settling during the crucial phase of matrix polymerization. This precise control over the position of the inclusion ensures integrity of the composite and allows customization of material properties to meet specific application.

Another novelty of the current work is the development of the hyperelastic-based material characterization of SLCs based on volume fraction of the liquid inclusions obtained from the experimental data. These data are currently not available in literature especially for the silicone matrix with Glycerin inclusion, to the best of the authors knowledge. Having precise hyperelastic data for various volume fractions are crucial for predicting analytically the mechanical behavior, stability, and durability of the composite under various conditions. Secondly, the availability of such data drastically reduces the development time which traditionally relies on generic or approximate values or by taking a more time-consuming method of experimenting and testing. Lastly, this study demonstrates how SLCs, crafted using this novel technique, can be used to fabricate biofidelic soft materials with properties mimicking natural biological tissues which are currently fabricated without the liquid inclusions [3].

Summary:

This chapter provides an introduction to solid-liquid composites (SLCs), followed by a review of existing studies on SLCs, their mechanical properties, challenges in fabrication of SLCs and the research objectives. SLCs are categorized into macro-structured (solid matrix infused with liquid) and micro-structured (homogeneous distribution of solid and liquid phases) depending on the distribution of the liquid phase. These composites can be used in diverse applications, including drug delivery, tissue engineering, thermal storage, sensing devices, actuators, flexible electronics, conductive applications, coatings, targeted drug delivery, and impact resistance. The choice of liquid medium, such as metallic, aqueous, hydrocarbons, silicones, fluorocarbons, and ionic liquids, impacts additional to the overall composite. Solid matrices, including silicones, polyurethanes,

and hydrogels, are selected based on compatibility, stiffness, extensibility, and other properties, offering excellent versatility for the development of SLCs.

Various experimental and analytical techniques have been explored to estimate the mechanical properties of SLCs, with a focus on hyperelastic material behavior. Experimental studies highlighted stiffening effects in soft matric with increased volume fraction of liquid inclusions of tiny sizes, while analytical models employing Eshelby's extension theory considered surface effects and capillary phenomena. However, limited research directly characterizes SLCs with soft polymeric matrices and liquid inclusions. Fabrication challenges, including the precise integration of liquid inclusions without surfactants, are discussed. The chapter introduces the innovative approach developed in this work to fabricate SLCs and its focus on hyperelastic-based material characterization, offering precise data for different volume fractions of liquid inclusions.

Chapter 2: Preparation and Methodology

The fabrication of solid-liquid composites is an intricate process involving multiple steps and methods. Various techniques were used using a trial-and-error approach at developing an optimum SLC fabrication technique. This chapter covers two sections, in the first section the study discusses the novel methodology proposed for the fabrication of SLCs using silicone matrix with Glycerin inclusion. The second section covers various other approach that were explored to fabricate and was not feasible, these details serve as a valuable learning exercise, shedding light on the hurdles faced, and the limitations encountered during the fabrication phase.

2.1 Proposed Fabrication Process:

A CAD model of the mold having dimensions 50 mm x 10 mm x 3 mm (1.5ml volume) for casting the SLC coupons was first developed using PTC-Creo 9.0 (Parametric Technology Corporation) and was 3D printed on QIDI X-max using polylactic acid (PLA) filament material.

Figure 5: Fabrication of SLC- step 1, CAD models and 3D printing.

Commercially available platinum-catalyzed silicone from Smooth-On Ecoflex 00-30 (super soft, batch number X001KK06WN) was used as the soft matrix, and laboratory grade Glycerin from Home Science Tools, (LOT AD-22327-3, CAS-No-56-81-5) was used as the liquid inclusion phase.

Silicone as the matrix phase had the unique property of mimicking certain biofidelic tissues (Chanda et al.) [3]; and hence, is considered as an ideal choice for the solid matrix. Glycerin was chosen due to its non-toxic property, wound healing properties, and being one of the common ingredients in food, cosmetics, and other biomedical applications [48], [49], [50]. Additionally, Glycerin is immiscible with silicone, meeting one of the important requirements for developing a SLC.

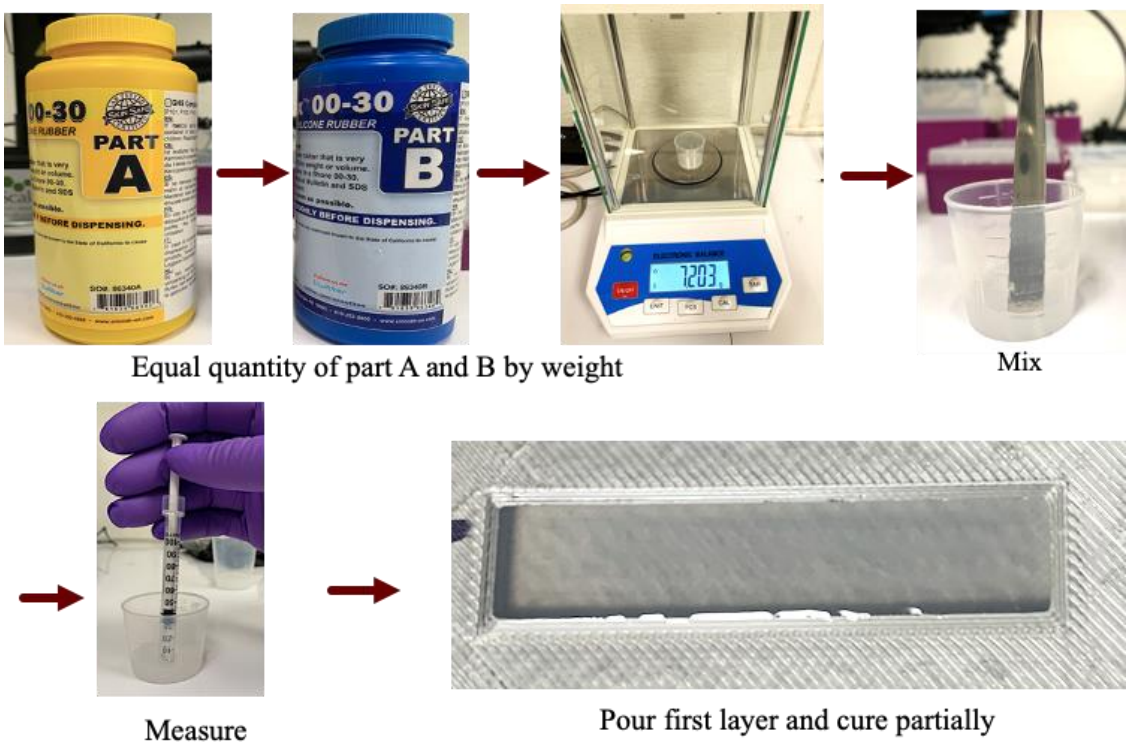

Figure 6: Fabrication of SLC- step 2, development of first layer.

The mold and the mixing cup were first cleaned with lint-free wipes using Iso-Propyl Alcohol, and Part-A and Part-B of Eco-flex 0030 were separately stirred for 250 rounds using separate stainless-steel rods. Utilizing a digital weighing scale, 10 grams of both Part-A and Part-B were poured into a cleaned cup, and the mixture was stirred using clean steel stirrer rods for another 250 rounds. Using a 1 mm diameter syringe, quantity 0.5 ml of the mixed solution was filled. The residual on the syringe openings was cleaned with lint-free wipes and the mixture from the syringe was poured onto the mold starting from the center of the cavity and extending to the entire length without reaching the edges. This step is very important because the solution when poured from the side walls would get attracted to the walls due to the surface tension effects and will result in an extremely thin layer at the center and thicker edges. The partially filled mold was left to partially cure for 2 hours on a flat surface at room temperature (70 – 72^0 F) (**Error! Reference source not found.**).

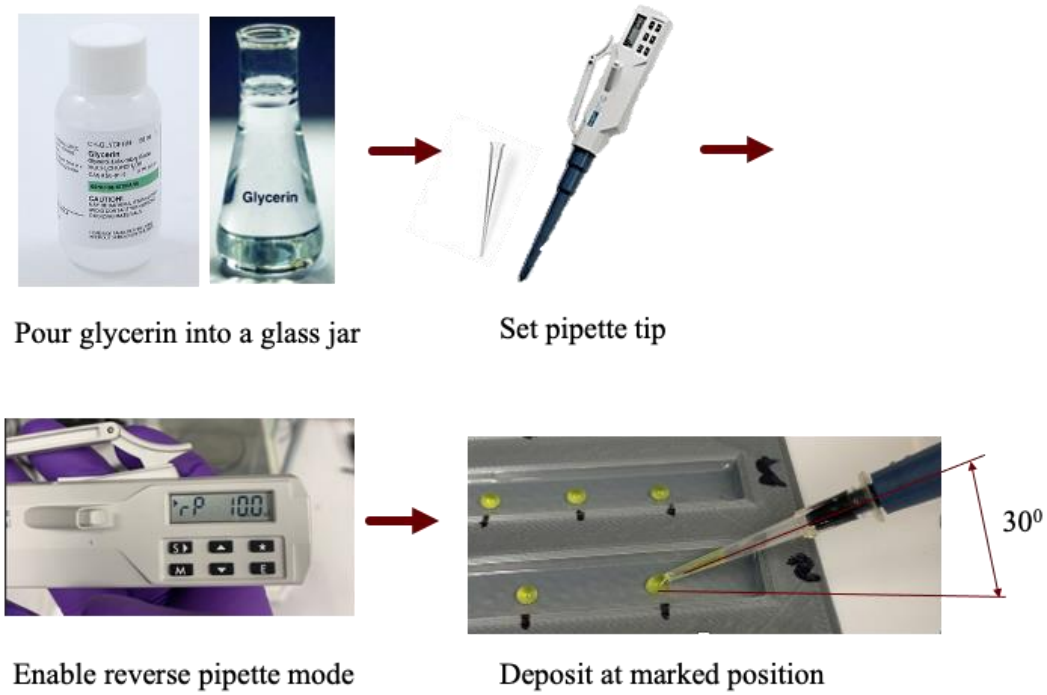

Figure 7: Fabrication of SLC- step 3, preparation of Glycerin inclusions.

The Glycerin bottle was mixed using a clean steel stirrer for 50 times, and approximately 5 ml of Glycerin was poured into a cleaned cup. A bio-hit pro-line 0.2-10 µL electronic pipette with a reverse pipette setting of 10 µL. was used to fill the Glycerin from the cup, any residual from the pipette tip was then cleaned using a lint-free wipe. The pipette was positioned to the pre-marked locations on the mold, and the actuator was pressed to release the Glycerin onto the prepared partially cured first layer of silicone. This step was mastered after a few trials and the pipette was oriented at an approximate angle of 30 degrees while releasing the droplets (Figure 7). Care was taken to prevent the tip from indenting the first layer of silicone (which was partially cured for 2 hours). This step was repeated for all the inclusions shown in Figure 8. The linear and staggered arrangements of Glycerin inclusions are shown in Figure 9.

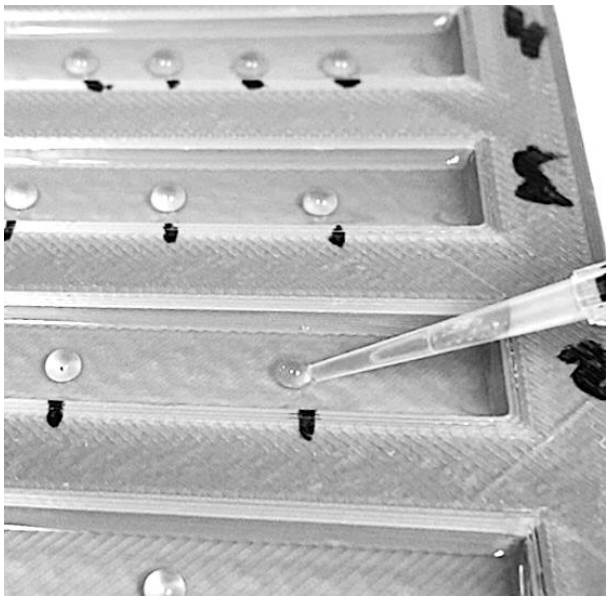

Figure 8: Fabrication of SLC- step 4, generation of Glycerin droplet.

Figure 9: Fabrication of SLC- step 5, arrangements of Glycerin inclusions (a) Showing linear arrangements (b) Showing staggered arrangements.

A fresh batch of silicone (Eco flex 0030) Part-A and Part-B were taken in a clean cup as previously mentioned and were stirred for 250 rounds using clean stainless-steel stirring rods and loaded onto a syringe with a 1 mm opening diameter. The mixture was poured into the partially loaded mold by surrounding the droplet first and then covering the top of the droplet. Various alternative pouring techniques were tried before selecting the current approach of enclosing the inclusion first. This particular approach effectively prevents the droplet from moving during the pouring of silicone. The filled mold was left on a flat surface to cure for 24 hours in a closed room at an ambient temperature (70 – 72^0 F) (Figure 10). Post 24 hours of curing, by wearing powder-free nitrile gloves, the samples were extracted from the mold in a slow, roll and peel method without applying excessive force or using any extraction tools. The extraction was ensured to be smooth without any silicone sticking to the surface of the cavities of the mold.

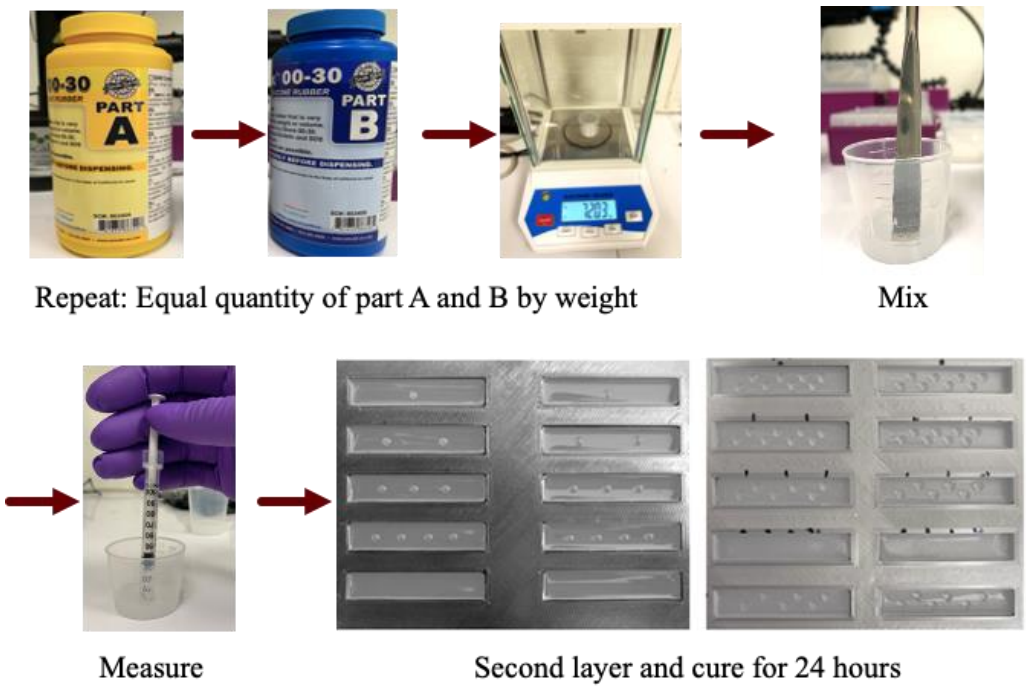

Figure 10: Fabrication of SLC- step 6, encapsulating the liquid inclusions and curing.

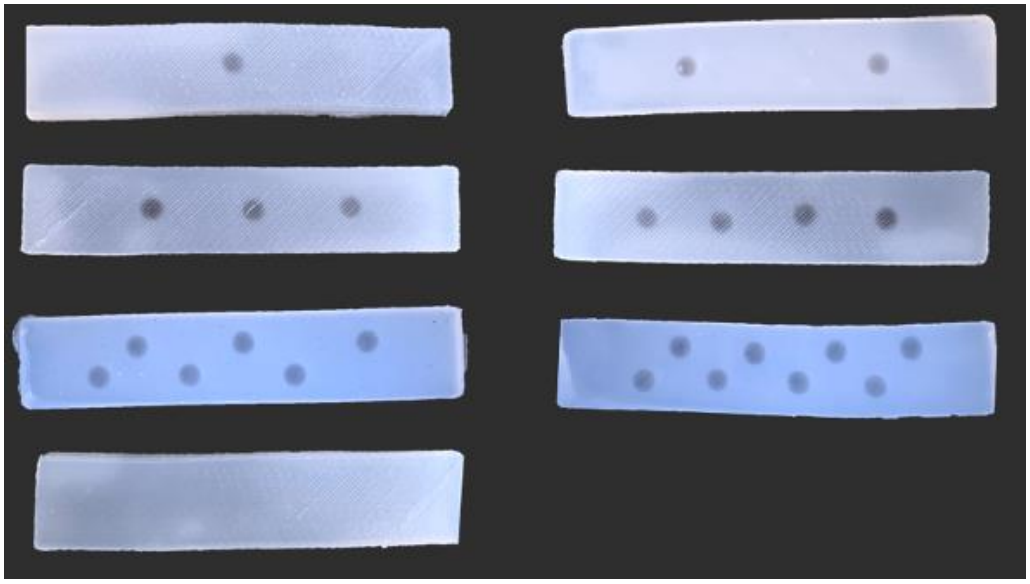

Figure 11: Showing extracted SLCs from the mold.

The extracted samples (Figure 11**Error! Reference source not found.**) were then inspected for air pockets and voids using bright light (Figure 12), the samples are bagged

and tagged for traceability. To prevent contamination, the samples were not touched with bare hands during extraction or testing.

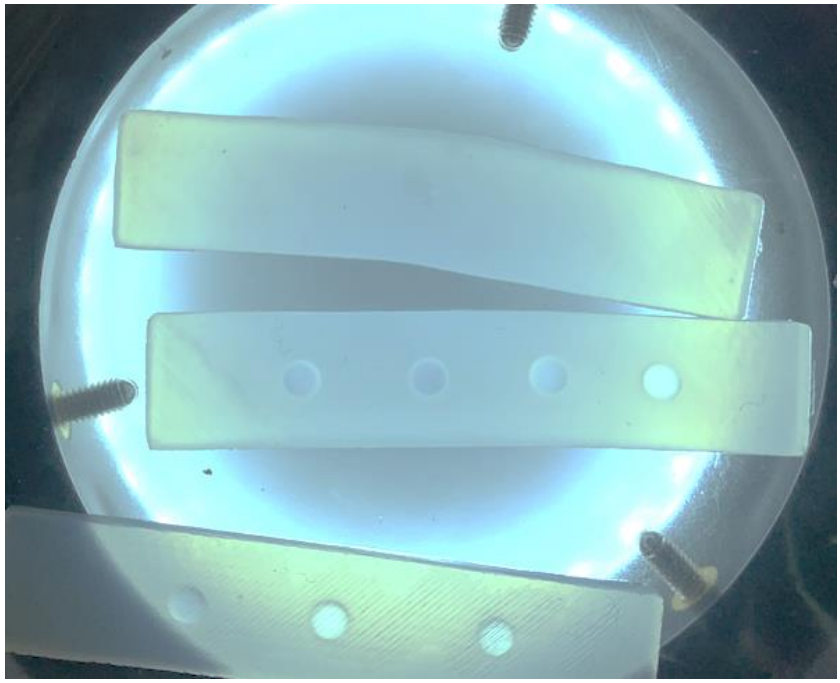

Figure 12: Inspection of SLCs under bright light.

2.2 Alternate Fabrication Methods Considered but not Pursued:

Several fabrication methods were explored to fabricate an SLC using silicone matrix and various types of liquid inclusions before finalizing a chosen technique. Each method had its unique set of challenges which are discussed below.

Injection method:

A silicone matrix was created using Smooth-On EcoFlex 0030. After curing for 24 hours, the matrix was carefully extracted from the mold and using a small syringe, inclusions were injected at predetermined locations (Figure 13). Water and Glycerin served as the inclusion medium. It was observed that injecting water was more

straightforward than injecting Glycerin. In both instances, however, the liquids seeped out once the syringe was removed. This seepage occurred because the needle created a permanent hole that did not close once withdrawn or after polymerization. Secondly, the silicone matrix functioned like a water-filled balloon upon injection of the inclusion. After the injection ceased and the syringe was removed, the material gradually shrunk back to its original state, pushing the inclusions out through the syringe hole.

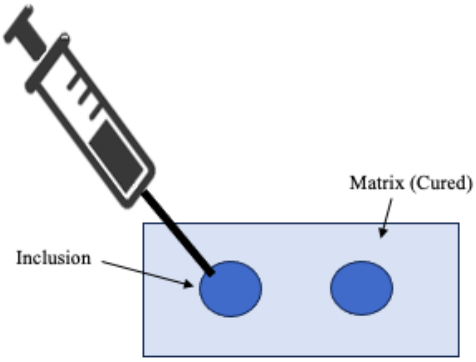

Figure 13: Schematic of an injection of a liquid inclusion into a cured matrix.

Homogeneous mixing:

In this approach, SLC was prepared with silicone matrix (Smooth-On EcoFlex 0030) loaded with inclusions of either water, Glycerin, antibacterial cream, or skin moisturizers. In separate experiments, each inclusion was thoroughly blended with silicone before being poured into a mold for curing. It was noted that water and Glycerin droplets tended to accumulate at the bottom of the mold during the curing process (Figure 14). However, the antibacterial cream and moisturizer exhibited a relatively more even distribution, but still tended to concentrate towards the bottom surface. Positioning the

liquids proved to be challenging, and controlling the size of the inclusions was not possible as it was evenly mixed with the silicone.

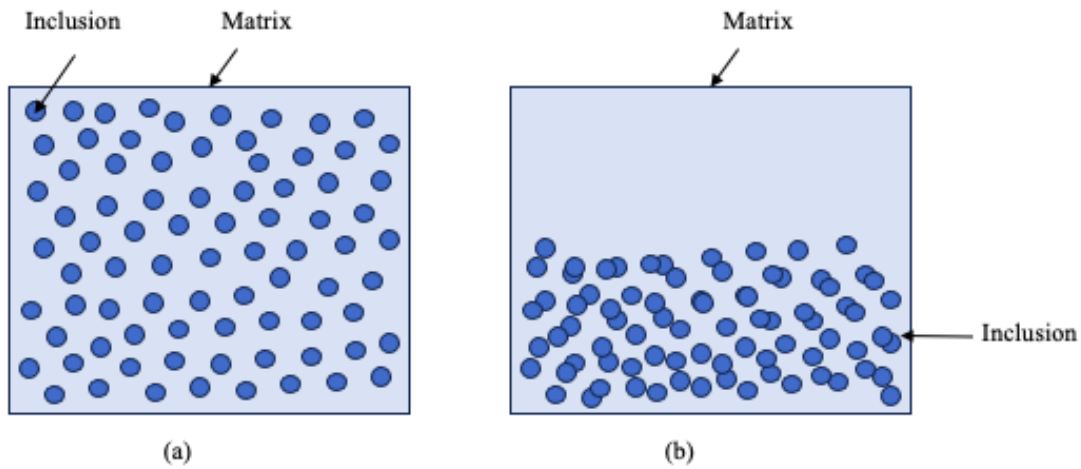

Figure 14: Schematic of polymerization process showing (a) inclusions in uncured matrix, (b) inclusions settling when cured.

Insertion molding:

In an alternate approach, a two-plate mold was developed to establish a dedicated space for the inclusions. The base plate included a cavity, while the top plate contained protrusions designed to produce circular impressions. The silicone was poured into the base plate and then the top plate was positioned, which enabled the circular protrusions to sink into the liquid silicone and create an impression upon partial curing.

While this method produced the desired circular impressions, two issues were encountered. Firstly, the liquid silicone matrix formed an extended wall around the round projections due to surface tension effects. Secondly, as the silicone matrix polymerized, it adhered to the inserts, resulting in the entire matrix being pulled out of the mold when attempting to separate the two halves. This unintended consequence created uneven,

miniature walls around the intended spaces meant for storing the inclusions (Figure 15). Hence, this method was not pursued further.

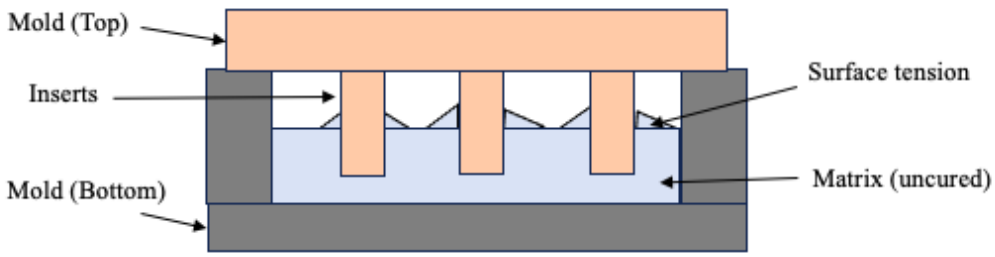

Figure 15: Schematic of rising polymer due to surface tension.

2.3 Experimental Setup:

UniVert CellScale mechanical testing system was used for uniaxial tension tests, and Univert software (ver-12.25) was used for data acquisition with a feature to capture images using a scientific camera (Figure 16). The scientific camera (accessory of CellScale) uses 2/3" CMOS image sensor to obtain a resolution of 2048 pixels by 2048 pixels. The load cell used with the equipment was a semiconductor strain gauge-based with an accuracy of 0.2% of the rated full-scale load up to 10N and has a unique calibration factor which is stored in a chip contained in the load cell connector. The load cell was calibrated using a known mass of 100 grams provided by the manufacturer. Holding fixtures were assembled before performing the calibration to prevent any post-calibration handling errors. Using a compression spring of known height provided by the manufacturer, the height between the platens were calibrated. The height was also independently validated using digital calipers. Due to the soft nature of the material, a low strain rate of 0.005 per second was used and the distance between the platens was set to 40 mm, providing 5 mm per edge space for clamping the sample. The total elongation

was set to 20 mm which corresponds to 50 percent strain, and the duration of each tensile test was set to 100 seconds followed by 5 seconds of unloading. The load cell data acquisition rate was set to 5 Hz.

The experimental stress-strain data of the pristine and the composite with various volume fractions of the liquid phases are used to determine the Young's Modulus, which is then compared with the theoretical formulations. In addition, the material constants for various hyperelastic formulations are also obtained from the experimental stress-strain curves, as discussed in the forthcoming sections.

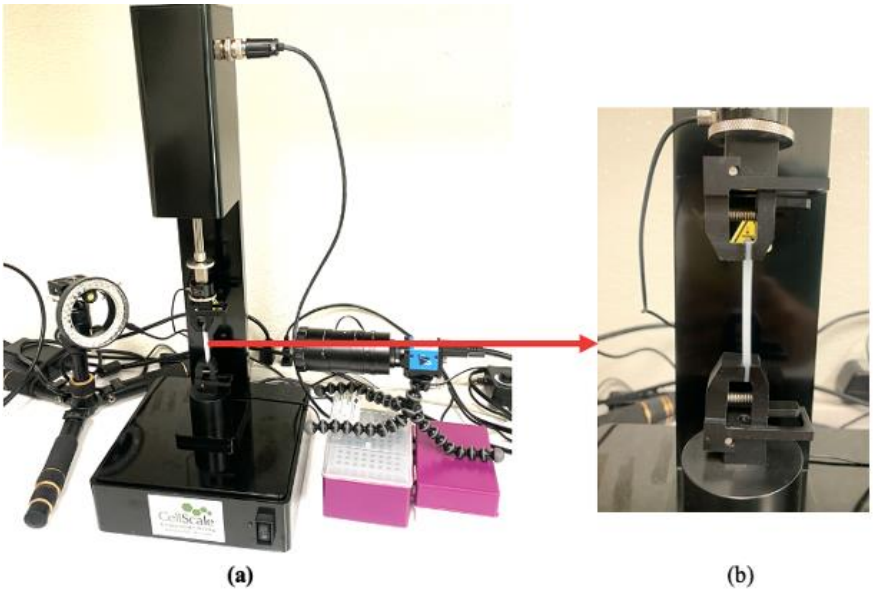

Figure 16: Schematic of testing equipment (UniVert CellScale) showing (a) Setup of uniaxial tensile test (b) Inset of setup showing a sample of SLC in the fixture.

Summary:

Chapter 2 outlines the various processes involved in the fabrication of solid-liquid composites (SLCs) with silicone matrix and Glycerin inclusions. The proposed fabrication method involves creating a mold using 3D printing, and then pouring a partially cured silicone layer into the mold. Glycerin droplets are strategically placed onto this layer using an electronic pipette. Another layer of silicone is then poured to enclose the droplets. The samples are allowed to cure for 24 hours and are extracted carefully. The chapter also discusses alternative methods that were explored, including injection methods, homogeneous mixing, and insertion molding, highlighting the challenges faced with each approach. The experimental setup for uniaxial tension tests using the UniVert CellScale mechanical testing system is detailed, with specific parameters mentioned, including strain rate, sample dimensions, and data acquisition rates. The stress-strain data from these experiments are used to determine Young's Modulus and hyperelastic material constants, providing valuable insights for further analysis.

Chapter 3: Effective Material Properties of the SLCs

Effective Young's Modulus:

The effective Young's Modulus of a composite represents the overall stiffness of the composite material and are influenced by the properties and amount of the individual phases. This parameter plays a critical role in materials engineering, aiding in the precise selection of composites for tailored applications. Eshelby's framework [51] is a widely used mathematical framework to understand the effect of inclusions or defects on the overall mechanical properties of a composite system. The effective stiffness of a solid containing dilute embedded mono-dispersed, in-compressible droplets is given by Eq.1 (refer [13]) where $\boldsymbol{\phi}$ is the volume fraction, $\boldsymbol{E}$ is the Modulus of elasticity of the matrix, and $\boldsymbol{E_c}$ is the effective Young's Modulus of the SLCs.

$$E_c = \frac{E}{1 + \frac{5\phi}{3}} \tag{1}$$

In composite material science, Eshelby's framework is foundational, but lacks consideration for the influence of surface stresses at the inclusion/matrix interface. Recent studies by Style et al. [13] involving nano-scale inclusions have shown the significant role played by surface stresses in defining the properties of soft solids. The importance was validated by both theoretical models and practical experiments [13].

Recognizing this gap, Style et al. [13] proposed an extension of Eshelby's theory by incorporating the effect of surface tension, which is contributing to the stiffening behavior within the composite. Considering surface tension becomes particularly relevant when the inclusion radius is smaller than the elastocapillary length, denoted as $\boldsymbol{L}$, in soft materials. $\boldsymbol{L} = \gamma/\boldsymbol{E}$, where γ is the surface tension of the liquid inclusion and **E** is the Young's Modulus of the matrix. Style's framework is given in Equation 2, where $\boldsymbol{\phi}$ is the volume fraction of the inclusion.

$$E_c = E\frac{1+\frac{5}{2}\frac{\Upsilon}{ER}}{\frac{5}{2}\frac{\Upsilon}{ER}(1-\phi)+\left(1+\frac{5}{3}\phi\right)} \tag{2}$$

While the above theory was mainly developed for dilute SLCs, Mancarella et al. [38] extended the Mori-Tanaka multiphase approximation scheme to incorporate the effect of inter-facial stresses in the non-dilute limit, to highlight the importance of accounting for surface tension effects. This study showed that composite stiffness depends strongly on the ratio of the droplet size $\boldsymbol{R}$, and the elastocapillary length scale, $\boldsymbol{L}$. Further, Mancarella et al. showed that the effective elastic Modulus of the composite stiffens when $\boldsymbol{R} < \boldsymbol{3L/2}$, and the extended framework is given in the Equation 3, for an incompressible matrix with Poisson's ratio $\boldsymbol{\nu} = ½$. Here $\boldsymbol{E_{rel}}$ is the effective Young's Modulus of the SLCs.

$$\mathrm{E_{rel}}\Big|_{\nu=\frac{1}{2}} = \frac{2-2\phi+\gamma'(5+3\phi)}{2+\frac{4}{3}\phi+\gamma'(5-2\phi)} \tag{3}$$

Hyperelastic characterization:

Most solid-liquid Composites with soft matrix phases exhibit hyperelastic material properties. These materials show highly non-linear stress-strain behavior. Unlike traditional materials, these composites undergo significant deformations under external forces, hence the use of a simple Modulus of Elasticity is inadequate for characterizing their effective properties [52].

Hyperelastic materials have a unique response to external mechanical loads, resulting in typically large strains and deformations. To understand and model this intricate behavior, numerous hyperelastic material models have been developed and discussed in literature [40]. These models provide valuable material information regarding the deformation responses.

Hyperelastic material models rely on the definition of the strain energy function, denoted by ψ and is dependent on the principal stretches ($\lambda_1, \lambda_2, \lambda_3$): $\psi = \psi(\lambda_1, \lambda_2, \lambda_3)$ or the Cauchy–Green tensor invariants $\psi = \psi(I_1, I_2, I_3)$ (see Equations 4,5,6) which are in turn functions of the principal stretches λ_i [3], [53]. If the material is isotropic, the strain energy function depends only on the three strain invariants, I_1, I_2, and I_3. If the hyperelastic material is also incompressible, the strain energy function can be written as a function of only two strain invariants, I_1 and I_2 [53].

From the engineering strains ($\varepsilon_{eng} = Extension\ (\triangle L)/Length\ (L)$) the engineering stretch relations λ_i can be extracted using $\lambda = 1 + \varepsilon_{eng}$, whereas engineering stresses is given by $\sigma = Load\ (F)/Area\ (A)$.

However, for an incompressible material: $\lambda_1 \times \lambda_2 \times \lambda_3 = 1$, and for uniaxial tension tests $\lambda_2^2 = (1/\lambda_1) = \lambda_3^2$. **[42]**

$$I_1 = \sum_{i=1}^{3} \lambda_i^2 \tag{4}$$

$$I_2 = \sum_{i,j=1}^{3} \lambda_i^2 \lambda_j^2 \quad i \neq j \tag{5}$$

$$I_3 = \Pi_{i=1}^{3} \lambda_i^2 \tag{6}$$

Using uniaxial test data of the samples, the principal Cauchy stress is expressed in terms of stretch and the strain energy function using Equation 7 [15].

$$\sigma_1 = \lambda_1 \frac{\partial \psi}{\partial \lambda_1} - \lambda_3 \frac{\partial \psi}{\partial \lambda_3}, \sigma_2 = \sigma_3 = 0 \tag{7}$$

Here, using the strain energy function, the stress vs stretch responses are curve fit for the following hyperelastic material models (using equations 8 -13).

i. neo-Hookean model.
ii. Mooney–Rivlin's 2-parameters.
iii. Mooney–Rivlin's 3-parameters.
iv. Mooney–Rivlin's 5-parameters.
v. Ogden's 2nd order.
vi. Ogden's 3rd order.
vii. Yeoh's 3rd order.

neo-Hookean Model:

The neo-Hookean model is a mathematical framework used to describe the elastic behavior of rubber-like and highly deformable materials that can undergo significant deformation while still retaining their elastic behavior (the ability to return to its original shape once the applied forces are removed). It is an extension of Hook's law for linear elasticity to include large deformations where the stress–strain relationship is nonlinear. [54]. The strain energy function is given in Equation 8, where $\boldsymbol{\mu}$ is the shear Modulus and $\boldsymbol{I_1}$ is the first principal invariant.

$$\Psi_{\text{neo}} = \frac{\mu}{2}\left(\overline{I_1} - 3\right) \tag{8}$$

Mooney–Rivlin model:

Mooney–Rivlin model is one of the popular models and is an extended form of the neo-Hookean model considering the second invariant term [40]. This model was formulated by Mooney and Rivlin and has a reputation for predicting the response of hyperelastic materials to a high level of accuracy [54]. The strain energy functions are given in Equations 9-11 respectively for Mooney–Rivlin's 2-parameters, 3-parameters, and 5-parameters models. Here, $\boldsymbol{I_1}$ and $\boldsymbol{I_2}$ are first and second strain invariants, and $\boldsymbol{C_{10}}$ and $\boldsymbol{C_{01}}$ are constants in the hyperelastic material model for the 2-parameter model, C_{10}, $\boldsymbol{C_{01}}$, and $\boldsymbol{C_{11}}$ are constants for the 3-parameter model and $\boldsymbol{C_{10}}$, $\boldsymbol{C_{01}}$, $\boldsymbol{C_{20}}$, $\boldsymbol{C_{11}}$, and $\boldsymbol{C_{02}}$, are constants for the 5-parameter models respectively.

$$\Psi_{\text{Mooney-2P}} = C_{10}\left(\overline{I}_1 - 3\right) + C_{01}\left(\overline{I}_2 - 3\right) \tag{9}$$

$$\Psi_{\text{Mooney-3P}} = C_{10}(\bar{I}_1 - 3) + C_{01}(\bar{I}_2 - 3) + C_{11}(\bar{I}_1 - 3)(\bar{I}_2 - 3) \tag{10}$$

$$\Psi_{\text{Mooney-5P}} = C_{10}(\bar{I}_1 - 3) + C_{01}(\bar{I}_2 - 3) + C_{20}(\bar{I}_1 - 3)^2 + C_{11}(\bar{I}_1 - 3)(\bar{I}_2 - 3) + C_{02}(\bar{I}_2 - 3)^2 \tag{11}$$

Ogden's model:

Ogden's model is used for characterizing the behavior of hyperelastic materials under large deformations and to account for nonlinear effects. This model is mostly used for characterization of biological tissues, under large deformations and to describe the mechanical behavior of a wide variety of materials with hyperelastic behavior [54]. The strain-energy function for Ogden's 2nd order and 3rd order models are given in Equation 12. Where $\boldsymbol{\mu}_i$ and $\boldsymbol{\alpha}_i$ are material parameters and $\boldsymbol{N}$ determines the number of material parameters, allowing the model to be adjusted for specific materials.

$$\Psi_{\text{Ogden}} = \sum_{i=1}^{N} \frac{\mu_i}{a_i} \left(\bar{\lambda}_1^{a_i} + \bar{\lambda}_2^{a_i} + \bar{\lambda}_3^{a_i} - 3 \right) \tag{12}$$

Yeoh's model:

Yeoh's model provides a more accurate representation of the material's behavior under various loading conditions. The strain-energy function for Yeoh's model depends only on the first strain invariant $\boldsymbol{I_1}$ [55] and is given in Equation 13, where $\boldsymbol{C_{i0}}$ are

constants. The Yeoh model is characterized by the parameter *N*, which determines the number of coefficients used in the model.

$$\Psi_{\mathrm{Yeoh}} = \sum_{i=1}^{N} C_{i0} \left(\bar{I}_1 - 3\right)^i \tag{13}$$

Summary:

Chapter 3 discusses the mathematical frameworks used to understand the mechanical properties of solid-liquid composites (SLCs). This chapter introduces Eshelby's framework, a fundamental concept in composite material science, which calculates the effective Young's Modulus of a composite considering the properties and volume fraction of individual phases. While Eshelby's framework forms the basis for the analytical characterization, recent studies have extended this theory to incorporate surface stresses at the inclusion/matrix interface, particularly important in soft materials. The chapter also discusses hyperelastic characterization, crucial for materials that undergo significant deformations. Various hyperelastic models are discussed, including the neo-Hookean model, Mooney-Rivlin models with different parameters, Ogden's models, and Yeoh's model.

Chapter 4: Results and Discussions[1]

Considering various factors that influence the formation of an optimum SLC, numerous fabrication methods were examined by evaluating the merits and demerits of each method. Notably, most existing methods involved intimately mixing the solid and liquid phases before polymerization, which lacks the ability to control the inclusion size and controlling the position of each inclusion. These methods involved the use of additives like surfactants to keep the liquid inclusions suspended. These surfactants will have some effect on overall material properties. Hence a novel methodology, without the reliance of surfactants, but with the ability to maintain the size and position of the liquid inclusion was developed.

As discussed in detail in chapter 2, commercially available silicone, specifically ECO-Flex 0030, was chosen as the matrix material, and Glycerin was selected as the preferred liquid inclusion. Samples of SLCs with various volume fraction of Glycerin inclusion was fabricated using unique process detailed in chapter 2, the fabrication method allowed precise control of inclusion position and size within the matrix. A total of 70 samples were prepared and tested.

[1] § Unnikrishnan, V.U., and K. Kundapur, "Elastomechanical Characterization and Novel Fabrication of Solid-Liquid Composites (SLCs) using Silicone matrix and Glycerin inclusions." Disclosure filed Sept. 12, 2023, Provisional patent application - 63/546,055 filed on Oct-27th-2023.

Experimental Studies:

Each sample of the pristine and SLCs with various volume fraction of the liquid phase was tested three times. The first test was performed when the samples were extracted from the mold after 24 hours of curing, the second test was carried out 24 hours after the first test, and the third test, 24 hours after the second test. These time intervals for testing were chosen to capture any changes in the material properties due to any subsequent polymerization. Two sets of samples were created for each volume fraction corresponding to 14 samples in one batch (refer table 1).

Table 1: Showing the number of samples in a batch & the corresponding volume fraction.

Number of 10 *µl* Inclusions	**Volume Fraction %**	**Number of samples**
0	0.00	2
1	0.82	2
2	1.62	2
3	2.35	2
4	3.08	2
6	4.70	2
8	6.16	2
	Total	14

The tests were conducted in 5 batches of 14 samples (i.e., 14 x 5 = 70 samples), and a total of 210 tests were conducted (70 samples x 3 tests = 210 tests). A space of 5 mm from the edge of the samples were marked using a felt pen, and this mark was used to position the samples on the experimental fixtures (Figure 17).

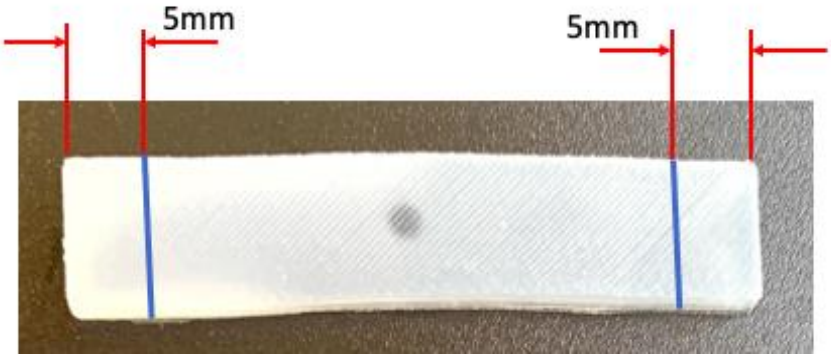

Figure 17: Showing the clamp area on one of the SLC samples.

The holding fixtures are made from plastic with knurling type serrations on the clamping area to prevent any slip. Multiple adjustments were made while clamping the samples to ensure no slack, this was a time-consuming and delicate task, a preload of 0.01 N was applied to keep preload consistency and to ensure minimum zero correction. The distance between the platens was finely adjusted within 40 (+/- 0.005) mm.

Each sample was carefully measured using a digital vernier caliper at multiple locations and average dimensions were recorded. Figure 18(a) shows the state of the liquid inclusion in the SLC before tensile loading was applied and the deformed shaped (at 50\% strain) of the inclusion is indicated in Figure 18(b). It can be clearly seen that there is no separation or voids formed at the interface between the silicone matrix and the liquid inclusion as shown in Figure 18(c). Finally, Figure 18(d) shows the state of liquid inclusion in the SLC, as the coupon returns to its original state upon unloading.

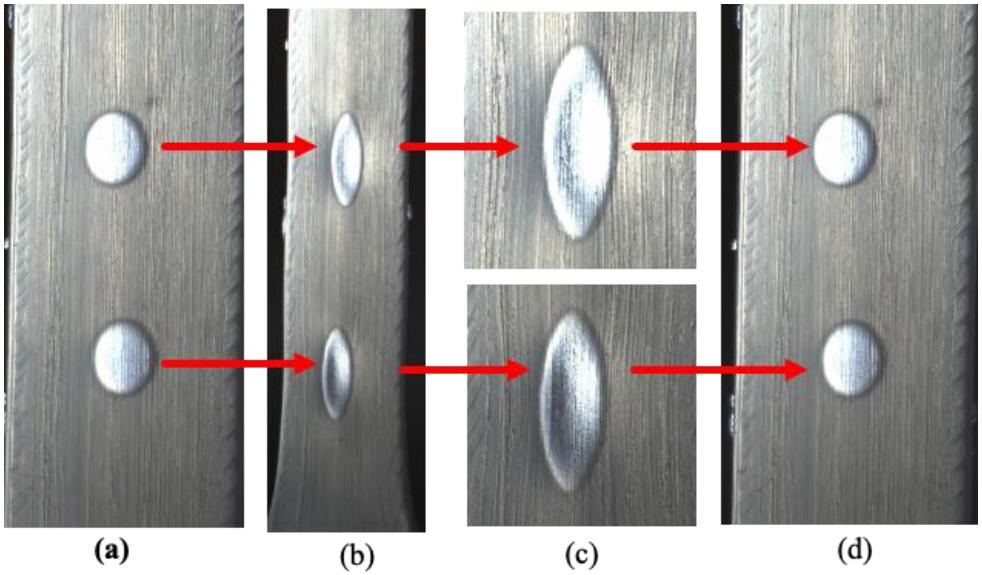

Figure 18: Schematic of Silicone-Glycerin SLC showing (a) In unstretched state, (b) Stretched state at 50% strain, (c) Inset of stretched SLC, (d) Unstretched state, SLC returned to its initial state.

The stress-strain data was plotted for each sample, Figure 19 shows stress-strain curves of one of the samples, which underwent 3 tests at a 24-hour interval.

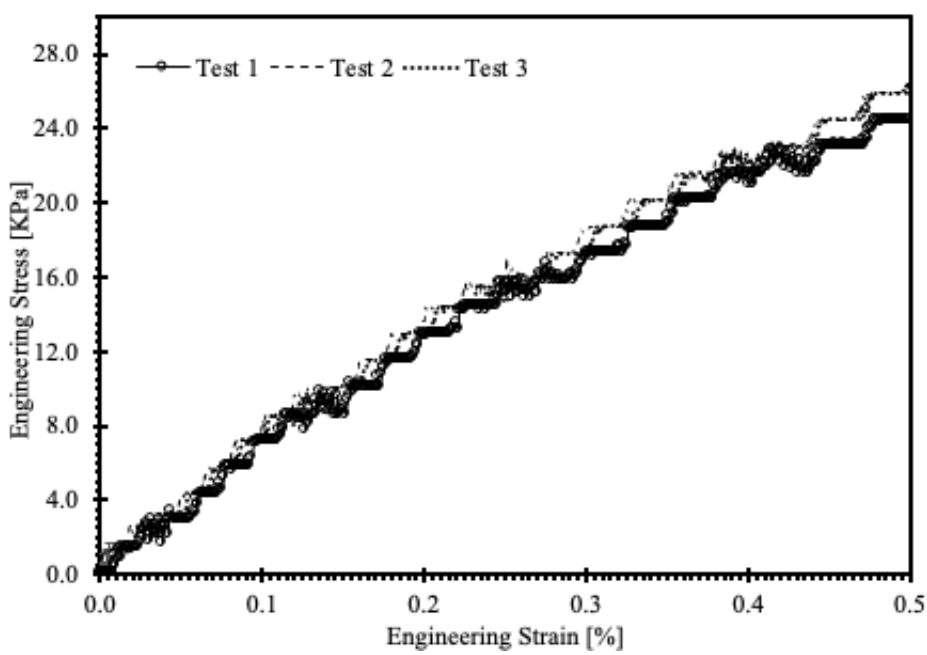

Figure 19: Showing the stress-strain plot for three tensile tests carried on one of the samples.

Average Young's Modulus was obtained from the slope of the stress-strain curves of each sample and the results are plotted for different volume fractions (0 to 6.16%) as shown in Figure 20.

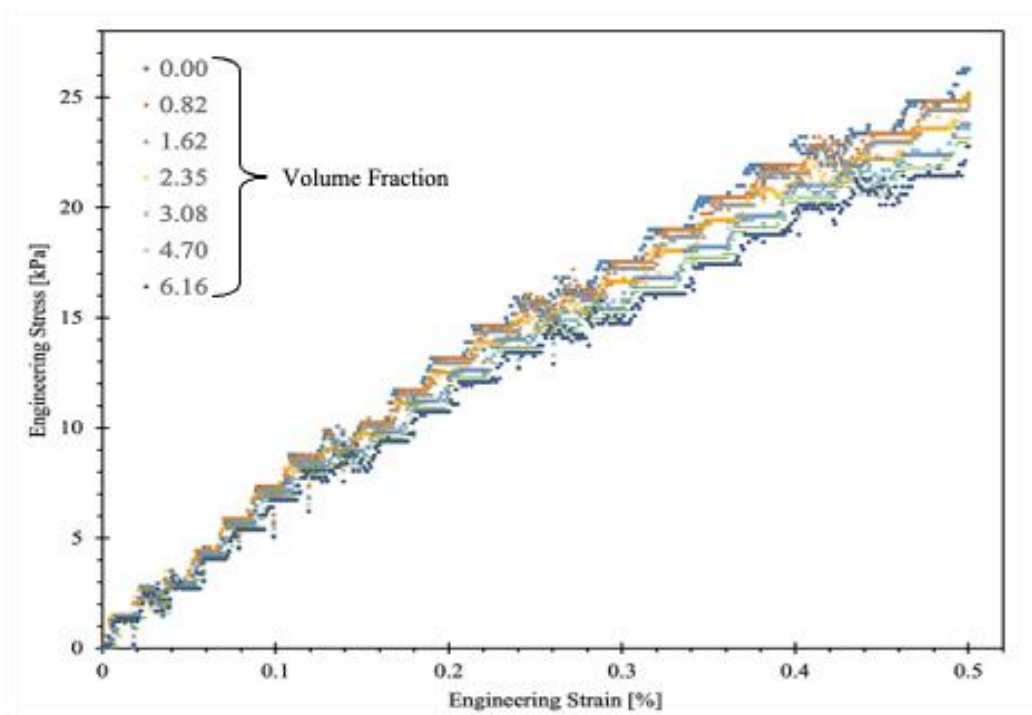

Figure 20: Showing average stress-strain data of the SLCs for varying volume fraction of the liquid phase.

The average Young's Modulus along with the standard deviation values for each of the volume fractions of the SLCs are indicated in Table 2, and it can be seen that there is a softening of the average Young's Modulus with an increase in the volume fraction of the liquid inclusions [13]. The average Young's Modulus of the fabricated SLCs also compares well with the range of elastic Modulus of human tissues (e.g. 25-260 kPa) [56].

Table 2: Showing the average Youngs's Modulus for various volume fractions of SLCs.

Number of 10 *μl* Inclusions	**Volume Fraction %**	**Avg. Modulus [kPa]**
0	0.00	56.5 ± 1.49
1	0.82	55.7 ± 1.57
2	1.62	54.4 ± 1.55
3	2.35	53.6 ± 1.48
4	3.08	51.6 ± 1.57
6	4.70	50.4 ± 1.47
8	6.16	49.0 ± 1.69

In Figure 21 the average Young's Modulus of the experimental data are compared with the stress-strain behavior of the biofidelic brain tissue surrogates from Chanda et al. [3], to highlight the fact that the developed SLCs exhibits behavior similar to a biofidelic material.

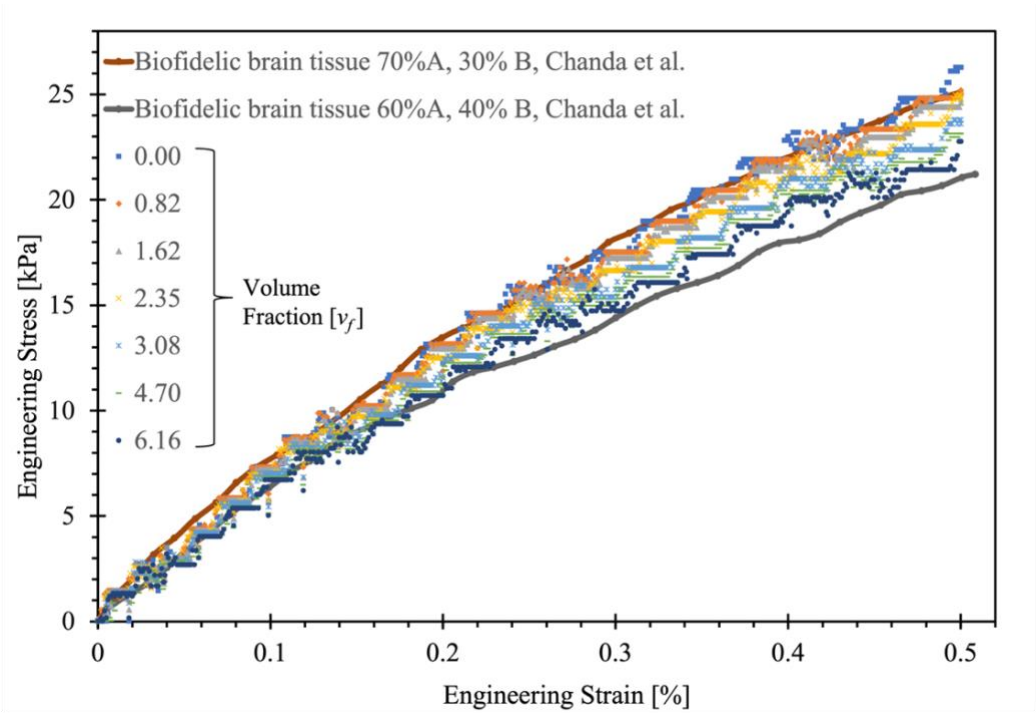

Figure 21: Showing average stress-strain data of the SLC for varying volume fraction of the liquid phase, compared with a biofidelic material data from literature.

The average Young's Modulus of the pristine matrix from the experimental data is 56.5 kPa (see Table 2), and using a measured inclusion radius of ***R=1.35mm*** and surface tension of Glycerin γ = 63.4 mN/m from literature [57], the effective Modulus of the SLC for various volume fractions of the liquid phase was obtained using the theoretical models by Eshelby's, Style's, and Manacerella's as discussed in chapter 3 (see Equations 1-3). These are compared with the experimental Young's Modulus as indicated in Figure 22.

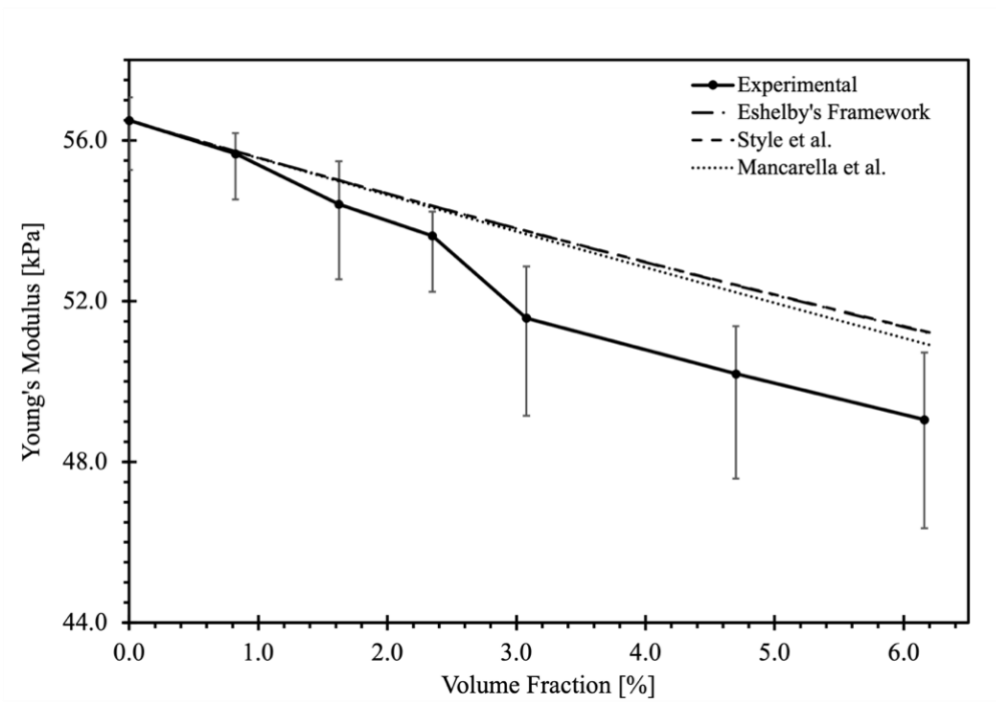

Figure 22: Showing the comparison of Young's Modulus with various micro-mechanical models.

It can be seen that the experimental Young's Modulus for lower volume fractions compares well with those of the analytical models, and the experimental studies by Mathias et al. [12]. However, it should be mentioned that the SLCs in Mathias et al. was fabricated using a uniform mix of the Glycerin inclusions. The experimental results start to deviate from the analytical models with an increase in volume fraction >3%, which is

attributed to the effect of staggered arrangement of the inclusions (Figure 9b) in the SLCs. As the inclusions gets closer, the inter-inclusion interactions increases, and these effects are not captured in the theoretical models.

Hyperelastic Material Parameters:

The experimental stress-strain data was now used for the characterization of SLCs using hyperelastic material models discussed in chapter 3. Curvefitter 2023 (Version 2.7.8480 by WelSim LLC) was used to determine the material constants for various volume fractions of the inclusion phase and are recorded in Table 3 to Table 9 along with the R^2 values for neo-Hookean, Mooney–Rivlin's 2-parameters, 3-parameters and 5-parameters, Ogden's 2nd order and 3rd order, and Yeoh's 3rd order models respectively. Notably, the R^2 values for different hyperelastic material models are between 0.984 to 0.996. Such a high R^2 value represents the high accuracy of the determined material constants. These hyperelastic material data are **not** currently available in literature for SLCs having silicone matrix with Glycerin inclusions and would be helpful in the development of computational models.

Table 3: Showing neo-Hookean material constant from the experimental stress-strain data.

Volume Fraction	neo-Hookean	
V_f	μ	R^2
0.00	24.8239	0.9932
0.82	24.5315	0.9939
1.62	24.0994	0.9941
2.35	23.8054	0.9951
3.08	22.8772	0.9940
4.70	22.3246	0.9955
6.16	21.5935	0.9940

Table 4: Showing the Mooney-Rivlin 2-parameter material constants from the experimental stress-strain data.

Volume Fraction	Mooney-Rivlin 2-parameters		
V_f	C_{10}	C_{01}	R^2
0.00	8.7083	5.0081	0.9961
0.82	8.9794	4.4438	0.9962
1.62	9.0482	4.0587	0.9960
2.35	10.0771	2.4686	0.9958
3.08	8.5787	3.8671	0.9959
4.70	9.6664	2.0228	0.9960
6.16	8.2915	3.3876	0.9957

Table 5: Showing the Mooney-Rivlin 3-parameter material constants from the experimental stress-strain data.

Volume Fraction	Mooney-Rivlin 3-parameters			
V_f	C_{10}	C_{01}	C_{11}	R^2
0.00	9.4881	4.1280	-0.2512	0.9961
0.82	10.1576	3.1142	-0.3796	0.9962
1.62	11.3365	1.4764	-0.7373	0.9960
2.35	16.7011	-5.0064	-2.1346	0.9961
3.08	10.6641	1.5138	-0.6719	0.9960
4.70	14.3508	-3.2634	-1.5094	0.9960
6.16	9.8553	1.6229	-0.5039	0.9958

Table 6: Showing the Mooney-Rivlin 5-parameter material constants from the experimental stress-strain data.

Volume Fraction	Mooney-Rivlin 5-parameters					
V_f	C_{10}	C_{01}	C_{20}	C_{11}	C_{02}	R^2
0.00	10.5823	3.2357	-48.2670	128.6220	-87.2145	0.9962
0.82	27.3725	-14.7658	-84.3061	237.1280	-177.1170	0.9960
1.62	35.7281	-23.8326	-122.1390	343.2030	-256.1130	0.9961
2.35	58.0779	-48.2511	-152.2990	435.7740	-337.3130	0.9962
3.08	37.0877	-25.9346	-126.8490	357.4320	-267.7780	0.9961
4.70	63.7931	-54.9144	-186.1010	532.6710	-410.3470	0.9960
6.16	46.4188	-36.1516	-211.9910	591.6990	-435.0710	0.9960

Table 7: Showing the Ogden's 2nd order material constants from the experimental stress-strain data.

Volume Fraction	Ogden's 2nd order				
V_f	μ_1	μ_2	a_1	a_2	R^2
0.00	153.9370	6.3412	0.2442	2.6206	0.9960
0.82	99.9235	10.3967	0.2990	2.2219	0.9962
1.62	25.0965	12.0894	1.3848	1.3832	0.9961
2.35	42.6397	0.0094	1.2635	7.80E-07	0.9847
3.08	32.1475	3.2156	1.3818	1.3851	0.9960
4.70	38.3516	1.93E-06	1.2606	0.0056	0.9950
6.16	24.1585	7.9339	1.4303	1.4312	0.9958

Table 8: Showing the Ogden's 3rd order material constants from the experimental stress-strain data.

Volume Fraction	Ogden's 3rd order						
V_f	μ_1	μ_2	μ_3	a_1	a_2	a_3	R_2
0.00	32.1133	5.9791	-0.8606	1.2855	1.3257	-6.4296	0.9961
0.82	19.8522	15.5959	-0.6651	1.4016	1.3975	-5.3627	0.9962
1.62	31.5458	2.4771	-2.3106	1.4638	1.2330	-1.0000	0.9960
2.35	46.4041	0.4671	-2.2939	1.0036	5.1925	-1.0000	0.9957
3.08	56.2126	2.4920	-2.0041	0.6935	3.3777	-1.0000	0.9956
4.70	50.7510	2.7793	-0.3069	0.7225	3.5791	-1.0000	0.9960
6.16	55.6907	1.2011	-0.1881	0.7418	4.1580	-1.0000	0.9957

Table 9: Showing the Yeoh's 3rd order material constants from the experimental stress-strain data.

Volume Fraction	Yeoh's 3rd order			
V_f	C_{10}	C_{20}	C_{30}	R_2
0.00	13.1923	-1.4986	0.5723	0.9960
0.82	12.9705	-1.3739	0.5501	0.9962
1.62	12.6325	-0.9801	0.2001	0.9960
2.35	12.1138	0.0894	-0.6534	0.9961
3.08	11.9982	-0.9535	0.2124	0.9959
4.70	11.3535	-0.0152	-0.0434	0.9961
6.16	11.2268	-0.5879	-0.0732	0.9957

***Summary**:*

Chapter 4 presents the results and discussions from experimental studies conducted on solid-liquid composites (SLCs). Various fabrication methods were explored, and a novel technique without surfactants, allowing precise control of inclusion size and position, was developed. The experiments involved fabricating 70 samples with different Glycerin volume fractions. Tensile tests were performed at 24-hour intervals on these samples,

capturing any changes in material properties due to subsequent polymerization. The average Young's Modulus of SLCs decreased with an increase in liquid inclusion volume fraction, showing softening behavior. The developed SLCs exhibited behavior similar to biofidelic materials, comparing well with the range of elastic Modulus of human tissues in the literature. Hyperelastic material models were applied, and material constants were determined for varying volume fractions, providing valuable data not available in the literature, and aiding in computational modeling efforts. The experimental results aligned well with analytical models for lower volume fractions, deviating for higher fractions due to inter-inclusion interactions, not considered in the theoretical models.

Chapter 5: Conclusions and Future Work

In this research, a new methodology for fabricating solid-liquid composites was established without using any additives (surfactants). The solid-liquid composites, composed of commercially available silicone Eco-Flex00-30 and laboratory-grade Glycerin, were fabricated using this novel technique, enabling accurate positioning of the inclusion phase within the composite system.

The silicone matrix of the SLC had the unique property of mimicking human brain tissues; hence, it was an ideal choice for the solid matrix. Glycerin was chosen due to its non-toxic properties and has been used in food, cosmetics, and other biomedical applications. Additionally, Glycerin is immiscible with silicone, meeting one of the important requirements for developing SLCs.

Three sets of uniaxial tests were conducted on each fabricated sample (discussed in chapter 4), totaling 240 tests on all the samples, covering liquid volume fractions from 0 to 6.16%. From the experimental stress-strain data, elastic moduli were established for all volume fractions. The experimental moduli were compared with various analytical theories (Eshelby's, Styles', and Manacerella's frameworks) discussed in chapter 4. For the volume fractions less than 3%, the experimental Young's Modulus matched well with those of the analytical models, consistent with studies conducted by Mathias et al.[12]. However, for the volume fractions above 3%, the experimental results start to deviate

from the analytical models, which may be attributed to the staggered arrangement of the inclusions (see Figure 9b) in the SLCs. It is assumed that as the inclusions get closer, inter-inclusion interactions increase, and these effects are not captured in the theoretical models.

An additional novelty of this work involves the development of a hyperelastic-based material model characterization of the fabricated composites with varying volume fractions of the liquid phase, especially for SLCs made of silicone and Glycerin combinations, these data are currently not available in the literature. In this study, hyperelastic material constants were established for neo-Hookean model, Mooney–Rivlin's 2-parameters, Mooney–Rivlin's 3-parameters, Mooney–Rivlin's 5-parameters, Ogden's 2nd order, Ogden's 3rd order, and Yeoh's 3rd order models; these data are presented in Tables 3 to 9.

It is also evident that the fabricated SLCs exhibit biomechanical properties similar to biofidelic materials in literature. The development of SLCs with precision in the position and amount of the liquid phase can ensure the applicability of the composite for various biomedical applications, where localized optimization and performance enhancements are necessary.

Future Work:

Future work involves characterizing the SLCs with different inclusion materials, and with various shapes and sizes of inclusions. A new fabrication process is being explored and

the samples will be characterized experimentally, analytically, and the corresponding hyperelastic parameters will be established accordingly.

Appendix: Research Outcomes

Intellectual Property Disclosure:

- Unnikrishnan, V.U., and K. Kundapur, "*Elastomechanical Characterization and Novel Fabrication of Solid-Liquid Composites (SLCs) using Silicone matrix and Glycerin inclusions*." Disclosure filed Sept. 12, 2023, Provisional patent application - 63/546,055 filed on Oct-27th-2023

Journal Publication:

- Kundapur, K., and V.U. Unnikrishnan, "*Elasto-mechanical Characterization and Novel Fabrication of Solid-Liquid Composites (SLCs) using Silicone matrix and Glycerin Inclusions*". Mechanics of Advanced Materials and Structures, 10.1080/15376494.2023.2282117. Accepted for publication on Nov-07-2023.

Technical Conferences:

- Kundapur, K., and V.U. Unnikrishnan, "*Computational Modeling and Size Effects of Sold Liquid Composites.*" Engineering Mechanics conference, June 6th-9th, 2023, Atlanta, GA.
- Unnikrishnan, V. U., and K. Kundapur, *"Elasto-mechanical Characterization of Liquid Reinforced Soft Solid Composites."* 2nd International Conference on Polymer Science and Engineering. Oct 30th - Nov 3rd, 2023, San Francisco, CA.

Poster Presentations:

- Kundapur, K., and V.U. Unnikrishnan, *"Computational modeling and size effects of Sold Liquid Composites.*" 18th Annual Faculty Poster Session and Research Fair, West Texas A&M University, March 2nd, 2023, Canyon, TX.

References

[1] S. Chen, H.-Z. Wang, R.-Q. Zhao, W. Rao, and J. Liu, "Liquid metal composites," *Matter*, vol. 2, no. 6, pp. 1446–1480, 2020.

[2] R. W. Style, R. Tutika, J. Y. Kim, and M. D. Bartlett, "Solid–liquid composites for soft multifunctional materials," *Advanced Functional Materials*, vol. 31, no. 1, p. 2005804, 2021.

[3] A. Chanda, C. Callaway, C. Clifton, and V. Unnikrishnan, "Biofidelic human brain tissue surrogates," *Mechanics of Advanced Materials and Structures*, vol. 25, no. 15–16, pp. 1335–1341, 2018.

[4] R. Hsissou, R. Seghiri, Z. Benzekri, M. Hilali, M. Rafik, and A. Elharfi, "Polymer composite materials: A comprehensive review," *Composite structures*, vol. 262, p. 113640, 2021.

[5] J.-H. Kruse *et al.*, "Polyoxometalate-Soft Matter Composite Materials: Design Strategies, Applications, and Future Directions," *Advanced Functional Materials*, vol. 32, no. 51, p. 2208428, 2022.

[6] D. Rus and M. T. Tolley, "Design, fabrication and control of soft robots," *Nature*, vol. 521, no. 7553, pp. 467–475, 2015.

[7] M. Yu, X. Li, P. Lv, and H. Duan, "Solid–Liquid Composites with High Impact Resistance," *Acta Mechanica Solida Sinica*, vol. 34, no. 6, pp. 911–921, 2021.

[8] H. Zhu *et al.*, "Anomalous scaling law of strength and toughness of cellulose nanopaper," *Proceedings of the National Academy of Sciences*, vol. 112, no. 29, pp. 8971–8976, 2015.

[9] P. S. Owuor *et al.*, "Nature inspired strategy to enhance mechanical properties via liquid reinforcement," *Advanced Materials Interfaces*, vol. 4, no. 16, p. 1700240, 2017.

[10] K. Lundon and K. Bolton, "Structure and function of the lumbar intervertebral disk in health, aging, and pathologic conditions," *Journal of orthopaedic & sports physical therapy*, vol. 31, no. 6, pp. 291–306, 2001.

[11] M. Humzah and R. Soames, "Human intervertebral disc: structure and function," *The Anatomical Record*, vol. 220, no. 4, pp. 337–356, 1988.

[12] K. A. Mathias, S. Hiremath, and S. Kulkarni, "Experimental studies on mechanical and dielectric behavior of Glycerol filled Silicone rubber composites," *Engineering Research Express*, vol. 3, no. 3, p. 035010, 2021.

[13] R. W. Style *et al.*, "Stiffening solids with liquid inclusions," *Nature Physics*, vol. 11, no. 1, pp. 82–87, 2015.

[14] Z. Sheng *et al.*, "Solid–liquid host–guest composites: The marriage of porous solids and functional liquids," *Advanced Materials*, vol. 33, no. 52, p. 2104851, 2021.

[15] A. Chanda, V. Unnikrishnan, K. Lackey, and J. Robbins, "Biofidelic conductive soft tissue surrogates," *International Journal of Polymeric Materials and Polymeric Biomaterials*, vol. 69, no. 2, pp. 127–135, 2020.

[16] N. Kazem, M. D. Bartlett, and C. Majidi, "Extreme toughening of soft materials with liquid metal," *Advanced Materials*, vol. 30, no. 22, p. 1706594, 2018.

[17] G. Faccio *et al.*, "Complete inclusion of bioactive molecules and particles in polydimethylsiloxane: a straightforward process under mild conditions," *Scientific reports*, vol. 9, no. 1, p. 17575, 2019.

[18] A. M. Vargason, A. C. Anselmo, and S. Mitragotri, "The evolution of commercial drug delivery technologies," *Nature Biomedical Engineering*, vol. 5, no. 9, pp. 951–967, 2021.

[19] H. Abdelkader *et al.*, "Polymeric long-acting drug delivery systems (LADDS) for treatment of chronic diseases: Inserts, patches, wafers, and implants," *Advanced drug delivery reviews*, vol. 177, p. 113957, 2021.

[20] X. Li, Y. Liu, Y. Xu, P. Tao, and T. Deng, "Solid–Liquid Phase Change Composite Materials for Direct Solar–Thermal Energy Harvesting and Storage," *Accounts of Materials Research*, 2023.

[21] G. Fredi, A. Dorigato, L. Fambri, and A. Pegoretti, "Multifunctional structural composites for thermal energy storage," *Multifunctional Materials*, vol. 3, no. 4, p. 042001, 2020.

[22] S. Wang, X. Zhao, J. Luo, L. Zhuang, and D. Zou, "Liquid metal (LM) and its composites in thermal management," *Composites Part A: Applied Science and Manufacturing*, p. 107216, 2022.

[23] Z. Shi *et al.*, "Morphological engineering of sensing materials for flexible pressure sensors and artificial intelligence applications," *Nano-Micro Letters*, vol. 14, no. 1, p. 141, 2022.

[24] E. Acome *et al.*, "Hydraulically amplified self-healing electrostatic actuators with muscle-like performance," *Science*, vol. 359, no. 6371, pp. 61–65, 2018.

[25] J. Yang *et al.*, "Ultrasoft liquid metal elastomer foams with positive and negative piezopermittivity for tactile sensing," *Advanced Functional Materials*, vol. 30, no. 36, p. 2002611, 2020.

[26] R. Tutika, A. T. Haque, and M. D. Bartlett, "Self-healing liquid metal composite for reconfigurable and recyclable soft electronics," *Communications Materials*, vol. 2, no. 1, p. 64, 2021.

[27] M. Yu, X. Li, P. Lv, and H. Duan, "Solid–Liquid Composites with High Impact Resistance," *Acta Mechanica Solida Sinica*, vol. 34, no. 6, pp. 911–921, 2021.

[28] R. C. Chiechi, E. A. Weiss, M. D. Dickey, and G. M. Whitesides, "Eutectic gallium–indium (EGaIn): a moldable liquid metal for electrical characterization of self-

assembled monolayers," *Angewandte Chemie International Edition*, vol. 47, no. 1, pp. 142–144, 2008.

[29] G. Cha, Y. S. Ju, L. A. Ahuré, and N. M. Wereley, "Experimental characterization of thermal conductance switching in magnetorheological fluids," *Journal of Applied Physics*, vol. 107, no. 9, 2010.

[30] Y. Wang, K. Li, X. Zhao, H. Tekinalp, T. Li, and S. Ozcan, "Toughening by nanodroplets: Polymer–droplet biocomposite with anomalous toughness," *Macromolecules*, vol. 53, no. 11, pp. 4568–4576, 2020.

[31] R. H. Ras and A. Marmur, *Non-wettable surfaces: theory, preparation and applications*. Royal Society of Chemistry, 2016.

[32] F. Malchiodi-Albedi *et al.*, "Biocompatibility assessment of silicone oil and perfluorocarbon liquids used in retinal reattachment surgery in rat retinal cultures," *Journal of Biomedical Materials Research: An Official Journal of The Society for Biomaterials, The Japanese Society for Biomaterials, and The Australian Society for Biomaterials and the Korean Society for Biomaterials*, vol. 60, no. 4, pp. 548–555, 2002.

[33] F. Ti, X. Chen, M. Li, X. Sun, S. Liu, and T. J. Lu, "Cylindrical compressible liquid inclusion with surface effects," *Journal of the Mechanics and Physics of Solids*, vol. 161, p. 104813, 2022.

[34] J. Wu, C. Ru, and L. Zhang, "An elliptical liquid inclusion in an infinite elastic plane," *Proceedings of the Royal Society A: Mathematical, Physical and Engineering Sciences*, vol. 474, no. 2215, p. 20170813, 2018.

[35] K. M. Hamdia and H. Ghasemi, "Quantifying the uncertainties in modeling soft composites via a multiscale approach," *International Journal of Solids and Structures*, vol. 256, p. 111959, 2022.

[36] P. Sharma and S. Ganti, "Size-dependent Eshelby's tensor for embedded nano-inclusions incorporating surface/interface energies," *J. Appl. Mech.*, vol. 71, no. 5, pp. 663–671, 2004.

[37] S. Krichen, L. Liu, and P. Sharma, "Liquid inclusions in soft materials: Capillary effect, mechanical stiffening and enhanced electromechanical response," *Journal of the Mechanics and Physics of Solids*, vol. 127, pp. 332–357, 2019.

[38] F. Mancarella, R. W. Style, and J. S. Wettlaufer, "Surface tension and the Mori–Tanaka theory of non-dilute soft composite solids," *Proceedings of the Royal Society A: Mathematical, Physical and Engineering Sciences*, vol. 472, no. 2189, p. 20150853, 2016.

[39] J.-H. Yun, Y.-J. Jeon, and M.-S. Kang, "Analysis of Elastic Properties of Polypropylene Composite Materials with Ultra-High Molecular Weight Polyethylene Spherical Reinforcement," *Materials*, vol. 15, no. 16, p. 5602, 2022.

[40] H. B. Khaniki, M. H. Ghayesh, R. Chin, and M. Amabili, "A review on the nonlinear dynamics of hyperelastic structures," *Nonlinear Dynamics*, vol. 110, no. 2, pp. 963–994, 2022.

[41] A. Weizel *et al.*, "Hyperelastic parameter identification of human articular cartilage and substitute materials," *Journal of the Mechanical Behavior of Biomedical Materials*, vol. 133, p. 105292, 2022.

[42] B. He, C. Zhang, Y. Zhou, and Z. Wang, "A computing method to determine the performance of an ionic liquid gel soft actuator," *Applied Bionics and Biomechanics*, vol. 2018, 2018.

[43] A. Chanda, V. Unnikrishnan, S. Roy, and H. E. Richter, "Computational modeling of the female pelvic support structures and organs to understand the mechanism of pelvic organ prolapse: a review," *Applied Mechanics Reviews*, vol. 67, no. 4, p. 040801, 2015.

[44] Y.-L. Park, C. Majidi, R. Kramer, P. Bérard, and R. J. Wood, "Hyperelastic pressure sensing with a liquid-embedded elastomer," *Journal of Micromechanics and Microengineering*, vol. 20, no. 12, p. 125029, Nov. 2010, doi: 10.1088/0960-1317/20/12/125029.

[45] K. Ghosh and O. Lopez-Pamies, "Elastomers filled with liquid inclusions: Theory, numerical implementation, and some basic results," *Journal of the Mechanics and Physics of Solids*, vol. 166, p. 104930, 2022, doi: https://doi.org/10.1016/j.jmps.2022.104930.

[46] S. Heyden, R. W. Style, and E. R. Dufresne, "Strain stiffening elastomers with swelling inclusions," *Soft Matter*, 2023.

[47] A. Abutaleb, D. Lolla, A. Aljuhani, H. U. Shin, J. W. Rajala, and G. G. Chase, "Effects of surfactants on the morphology and properties of electrospun polyetherimide fibers," *Fibers*, vol. 5, no. 3, p. 33, 2017.

[48] E. I. Stout and A. McKessor, "Glycerin-based hydrogel for infection control," *Advances in wound care*, vol. 1, no. 1, pp. 48–51, 2012.

[49] M. Savini, C. Cecchini, M. C. Verdenelli, S. Silvi, C. Orpianesi, and A. Cresci, "Pilot-scale production and viability analysis of freeze-dried probiotic bacteria using different protective agents," *Nutrients*, vol. 2, no. 3, pp. 330–339, 2010.

[50] P. Kalustian, "Pharmaceutical and cosmetic uses of palm and lauric products," *Journal of the American Oil Chemists' Society*, vol. 62, no. 2, pp. 431–433, 1985.

[51] J. D. Eshelby, "The determination of the elastic field of an ellipsoidal inclusion, and related problems," *Proceedings of the royal society of London. Series A. Mathematical and physical sciences*, vol. 241, no. 1226, pp. 376–396, 1957.

[52] M. Shahzad, A. Kamran, M. Z. Siddiqui, and M. Farhan, "Mechanical characterization and FE modelling of a hyperelastic material," *Materials research*, vol. 18, pp. 918–924, 2015.

[53] P. Martins, R. Natal Jorge, and A. Ferreira, "A comparative study of several material models for prediction of hyperelastic properties: Application to silicone-rubber and soft tissues," *Strain*, vol. 42, no. 3, pp. 135–147, 2006.

[54] S. K. Melly, L. Liu, Y. Liu, and J. Leng, "A review on material models for isotropic hyperelasticity," *International Journal of Mechanical System Dynamics*, vol. 1, no. 1, pp. 71–88, 2021.

[55] C. Renaud, J.-M. Cros, Z.-Q. Feng, and B. Yang, "The Yeoh model applied to the modeling of large deformation contact/impact problems," *International Journal of Impact Engineering*, vol. 36, no. 5, pp. 659–666, 2009.

[56] A. Kalra, A. Lowe, and A. Al-Jumaily, "Mechanical behaviour of skin: a review," *J. Mater. Sci. Eng*, vol. 5, no. 4, p. 1000254, 2016.

[57] K. Takamura, H. Fischer, and N. R. Morrow, "Physical properties of aqueous glycerol solutions," *Journal of Petroleum Science and Engineering*, vol. 98, pp. 50–60, 2012.